RESEARCH ARTICLE

Figures and figure supplements

Redefining innate natural antibodies as important contributors to anti-tumor immunity

Kavita Rawat *et al*

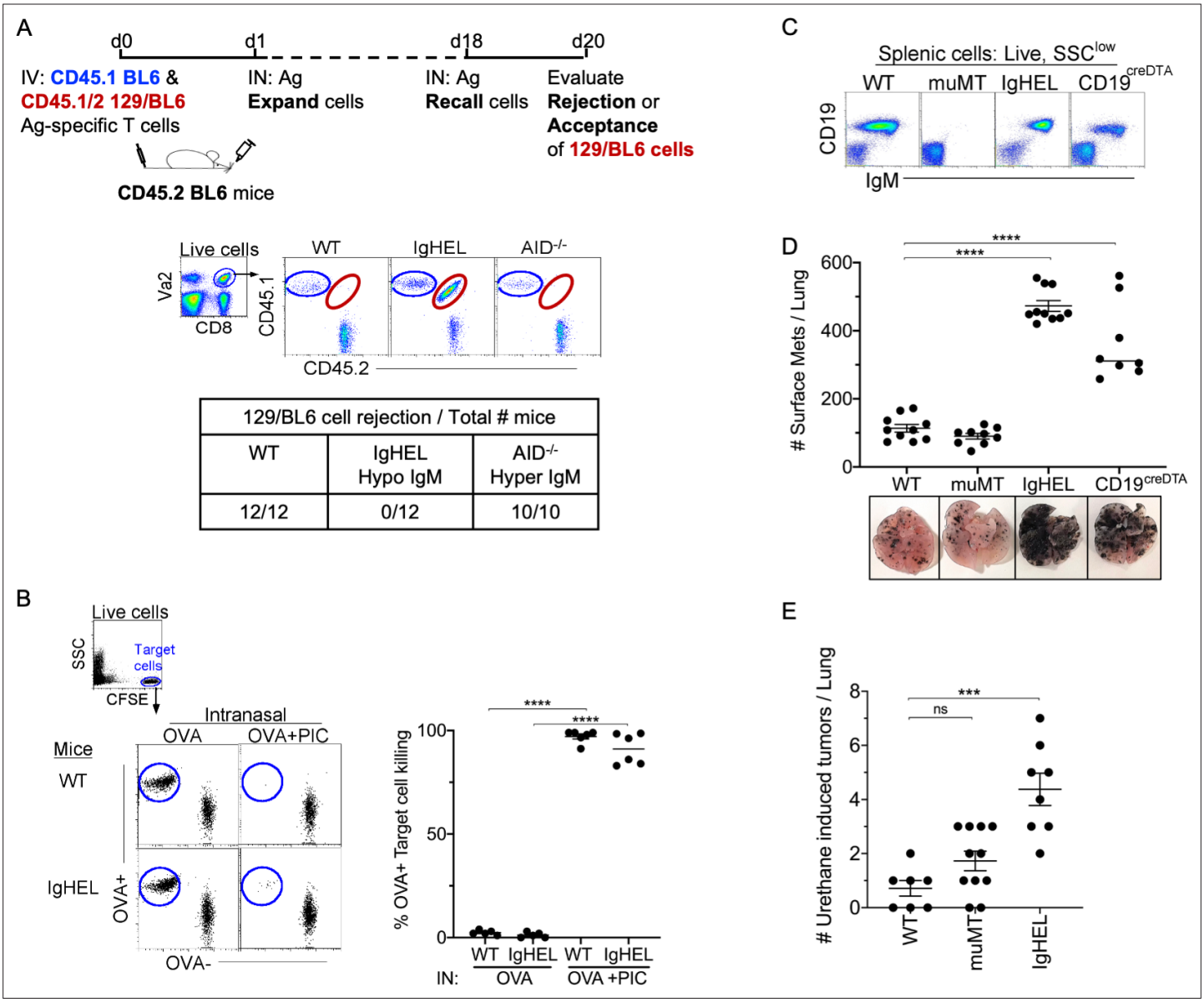

Figure 1. NAb repertoire is required for elimination of neoantigen expressing cells in absence of PAMPs. (**A**) *Experimental design*—Splenocytes from CD45.1 BL6-OT-I (internal control) and CD45.1/2 129BL6-OT-I were adoptively transferred into CD45.2 WT, IgHEL, and *Aicda* mice followed by i.n. delivery of OVA (Ag), which expands the cells expressing 129 neoantigens for detection in BL6 host. The mice were rechallenged with OVA on day 18 to assess 129BL6 cell rejection at day 20. Table illustrates # rejected/mice examined. (**B**) WT and IgHEL mice were instilled with 2 µg of OVA alone or with 10 µg of poly I:C. At day 6, CFSE-labelled OVA^- and OVA^+ target cells were transferred and assessed killing at day 8. Flow illustrates $CFSE^+$ target cells plotted as OVA^+ and OVA^- cells. Dots represent the number of mice. (**C**) Flow analysis of circulating lymphocytes in WT, muMT, IgHEL, and $CD19^{creDTA}$ mice plotted as CD19 versus IgM (**D**) WT, muMT, IgHEL, and $CD19^{creDTA}$ mouse lungs were inflated 16 days after i.v. B16F10 challenge. Pics depict total surface metastases (mets) per lung, which were enumerated and illustrated by scatter plot, each dot represents one mouse. Combined data of two independent experiments with 4–5 mice per group. ****p<0.0001. (**E**) WT, IgHEL, and muMT mouse lungs were inflated 6 months after urethane injections (***Figure 1—figure supplement 1B***). Scatter plot, each dot represents one mouse. ***$p<0.0001$, ns-non significant, mean ± SEM. NAb, natural antibody; PAMP, pathogen-associated molecular pattern; WT, wild-type.

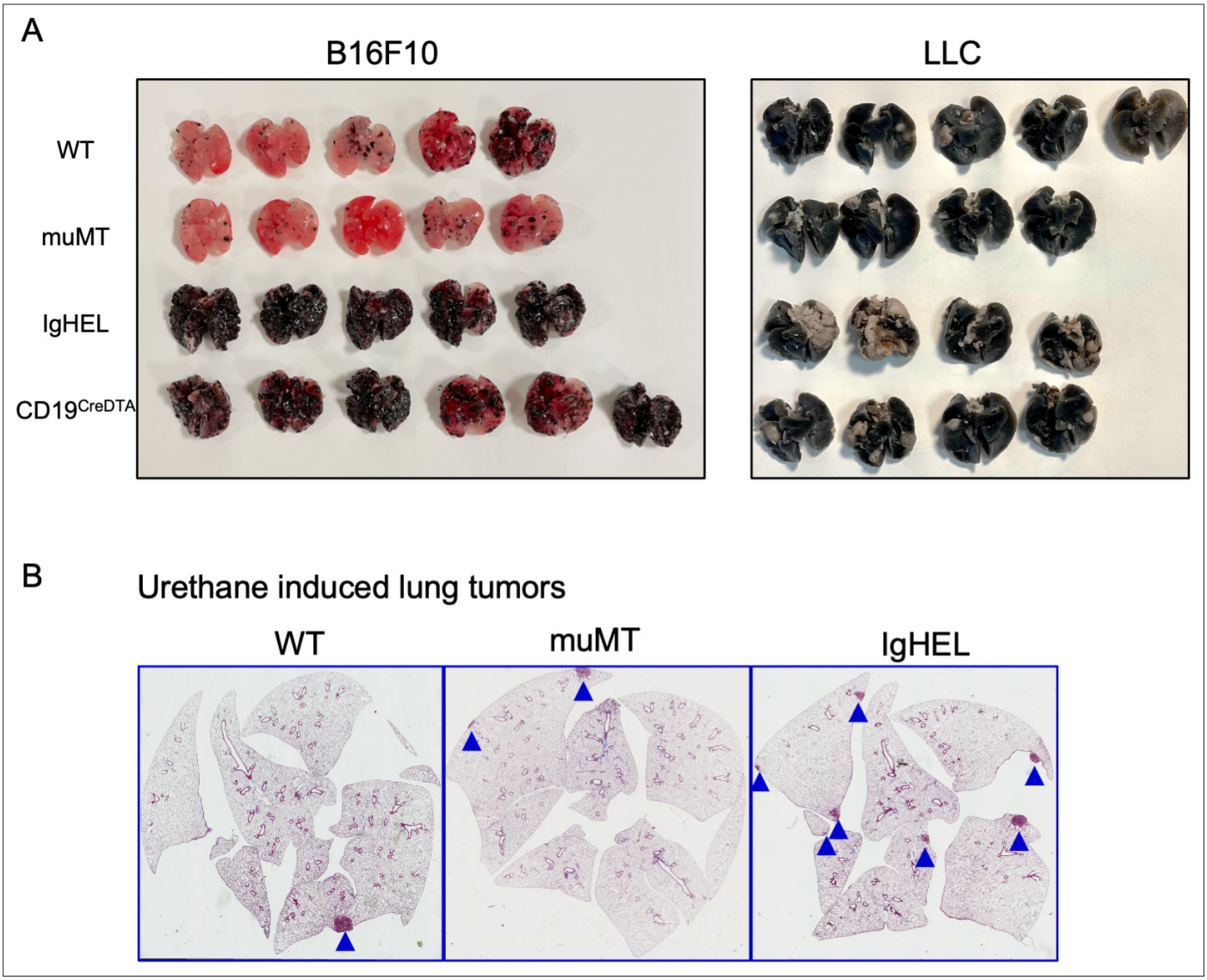

Figure 1—figure supplement 1. Tumor burden is greater in antibody-deficient mice. (**A**) B16F10 melanoma and Lewis lung carcinoma (LLC) tumor burden in WT, muMT, IgHEL, and $CD19^{CreDTA}$ female mice. Picture depicts agarose inflated lungs challenged with B16F10 melanoma in WT, muMT, IgHEL, and $CD19^{CreDTA}$ mice. Data represent two independent experiments with 4–5 mice per group. (**C**) Six months post urethane treated, IHC from WT, muMT, and IgHEL mice. Data represent IHC slides from individual mice, scatter plot in ***Figure 1E***. IHC, immunohistochemistry; WT, wild-type.

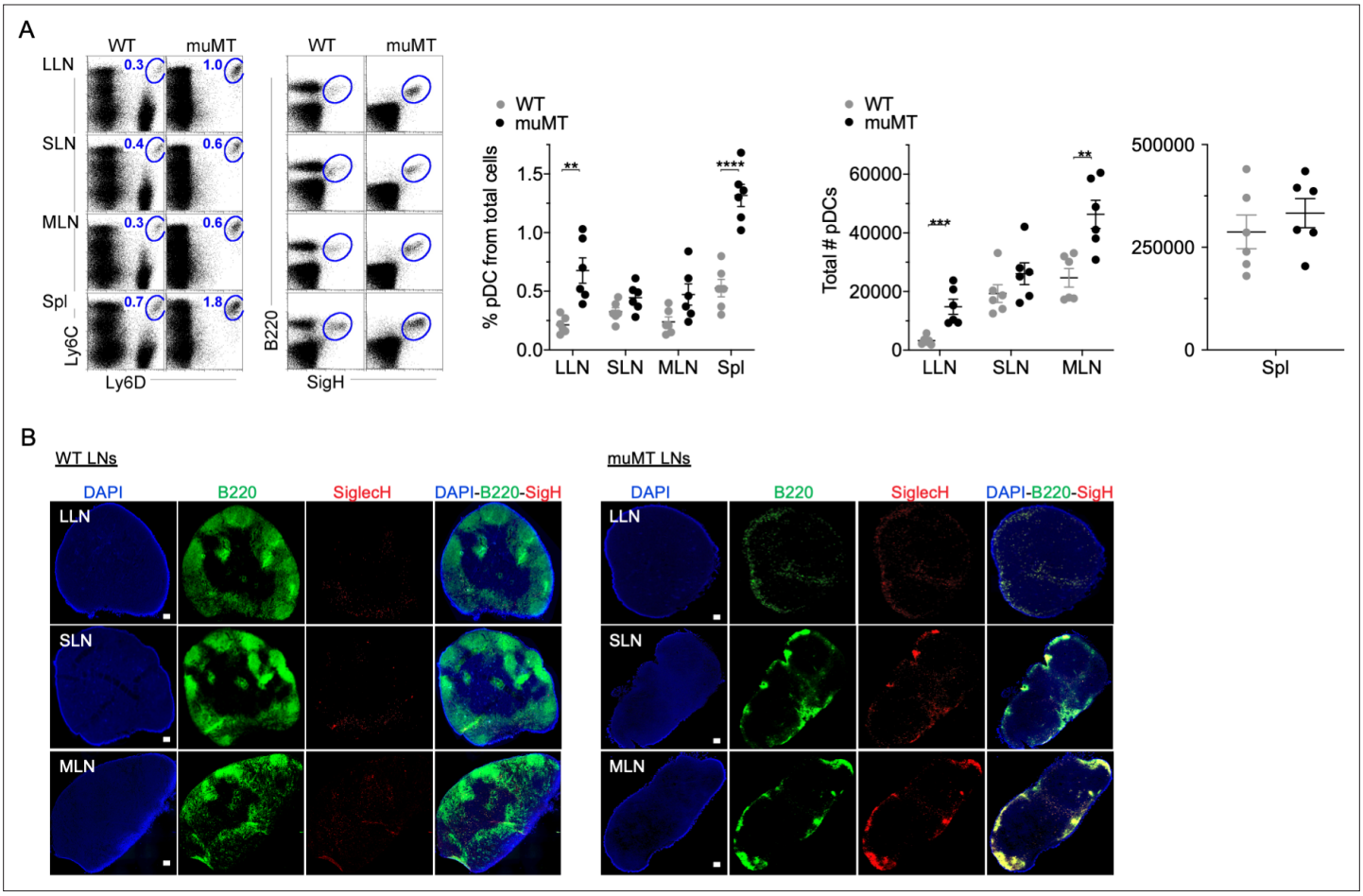

Figure 2. muMT mice have elevated levels of pDCs in lymph nodes and spleen. (**A**) Left, flow cells plotted as Ly6C versus Ly6D and B220 versus SiglecH to identify pDCs from B cells in lung draining-LNs (LLN), skin draining-LNs (SLN), mesenteric draining-LNs (MLN), and Spleen (Spl). Right, scatter plot displays the pDC frequency and count in WT and muMT mice. Data are representative two combined out of four independent experiments with 3 mice per group. **p<0.0097, ****p<0.0001, Gating strategy, ***Figure 2—figure supplement 1***. (**B**) IHC of LLN, SLN, and MLN from naïve WT and muMT mice. Sections were stained with DAPI (blue), anti-B220 (green), and anti-SiglecH (red). Scale bars, 100 μm. Data are representative of three independent experiments. IHC, immunohistochemistry; pDC, plasmacytoid dendritic cell; WT, wild-type.

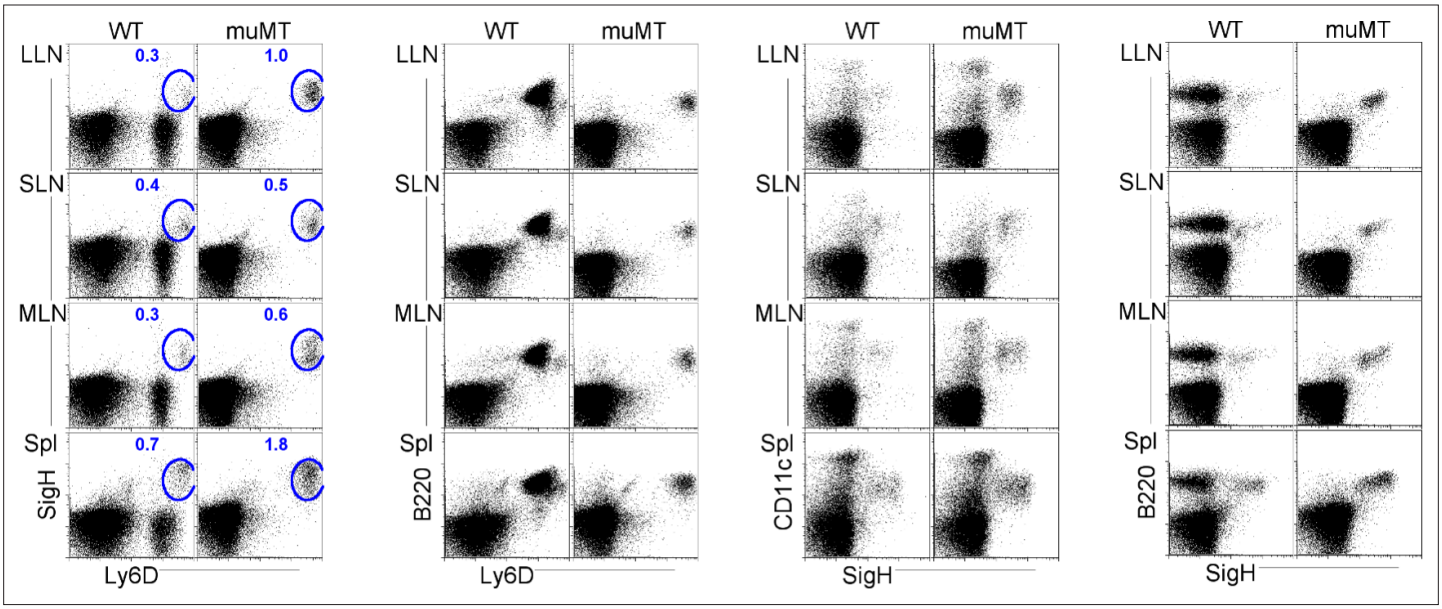

Figure 2—figure supplement 1. Flow plots illustrate pDC stains and gating strategies. Flow cells plotted in different ways such as SiglecH versus Ly6D, B220 versus Ly6D, CD11c versus SiglecH, and B220 versus SiglecH to identify pDCs in lung draining-LNs (LLN), skin draining-LNs (SLN), mesenteric draining-LNs (MLN), and Spleen (Spl). pDC, plasmacytoid dendritic cell.

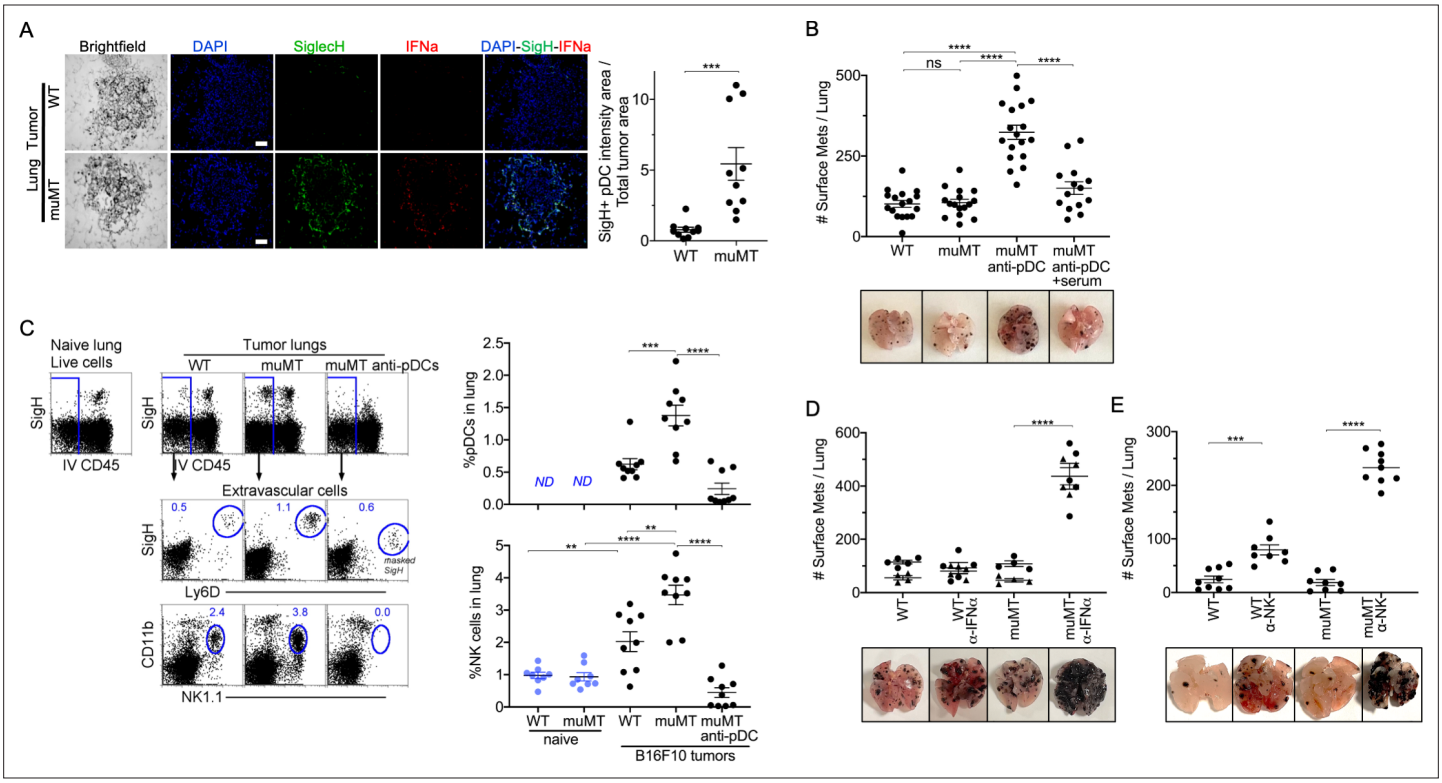

Figure 3. Depletion of pDCs in muMT mice results in increased tumor burden and decreased infiltration of NK cells at the tumor site. (**A**) IHC of lung B16F10 melanoma in WT and muMT mice stained with DAPI (blue), anti-SiglecH (green), and anti-IFN-α (red). Scale bars, 40 μm. Scatter plot illustrates Keyence quantitative software analysis of SigH$^+$ intensity over total tumor area×100. Each dot plot represents one random tumor analyzed per mouse from 5 mice per group. Data are representative of three independent experiments. (**B**) WT and muMT mouse lungs were inflated 16 days after i.v. B16F10 melanoma cell. Pics depict total surface metastases (mets) per lung, which were enumerated and illustrated by scatter plot, each dot represents one mouse. Two muMT groups were pDC-depleted, one group was given naive WT serum. Combined data of three independent experiments with 4–5 mice per group. ****p<0.0001. Non-significant (ns). Mean ± SEM. Anti-pDC treatment—***Figure 3—figure supplement 2***. Tumor burden—***Figure 3—figure supplement 3***. (**C**) At day 16, B16F10 tumor-induced WT and muMT mice were iv injected with anti-CD45 before harvesting, to exclude intravascular cells. Gating strategy: Top row, flow plots, gated on live cells followed by extravascular cell analysis (negative cells, iv CD45) in the naive and tumor-bearing lungs. Tumor cells plotted in second and third rows were gated on pDCs, SiglecH$^+$Ly6D$^+$, and NK cells CD11b$^+$NK1.1$^+$. Right, scatter plots display the pDCs and NK cell frequency in tumors of WT and muMT **p<0.0040, ***p<0.0077, ****p<0.0001, *ND* (not detected). Anti-pDC treatment—***Figure 3—figure supplement 2***. (**D**) Pics depict total surface metastases (mets) per lung in WT and muMT mice with and without anti-IFN-α treatment, each dot represents one mouse. ****p<0.0001, mean ± SEM. (**E**) Scatter plot represents individual mice from WT and muMT mice treated with and without anti-NK1.1. **p<0.001, ****p<0.0001, mean ± SEM. Data combined from two independent experiments with 3–5 mice per group. IHC, immunohistochemistry; pDC, plasmacytoid dendritic cell; WT, wild-type.

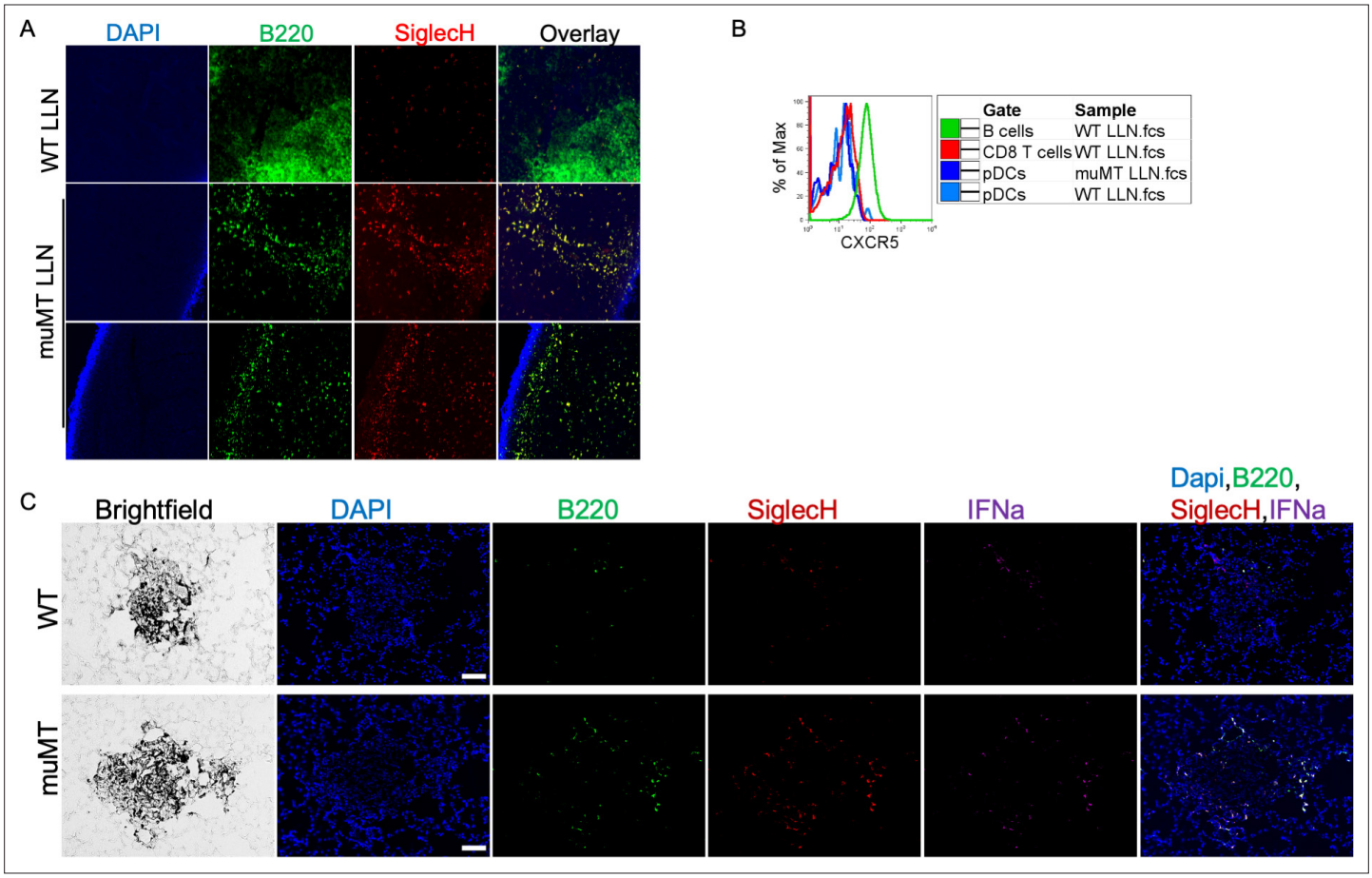

Figure 3—figure supplement 1. pDC staining of WT and muMT lymph nodes and lung tumors. (**A**) IHC 20× image muMT of LLN and Spl sections were stained with DAPI (blue), anti-B220 (green), and anti-SiglecH (red). Scale bars, 10 μm. (**B**) Histogram overlay showing the CXCR5 expression on immune cells isolated from WT and muMT mouse lung draining LNs (LLN). (**C**) IHC of lung melanoma in WT and muMT mice stained with DAPI (blue), anti-SiglecH (green), and anti-IFNa (red). Scale bars, 40 μm. Data are representative of three independent experiments. IHC, immunohistochemistry; pDC, plasmacytoid dendritic cell; WT, wild-type.

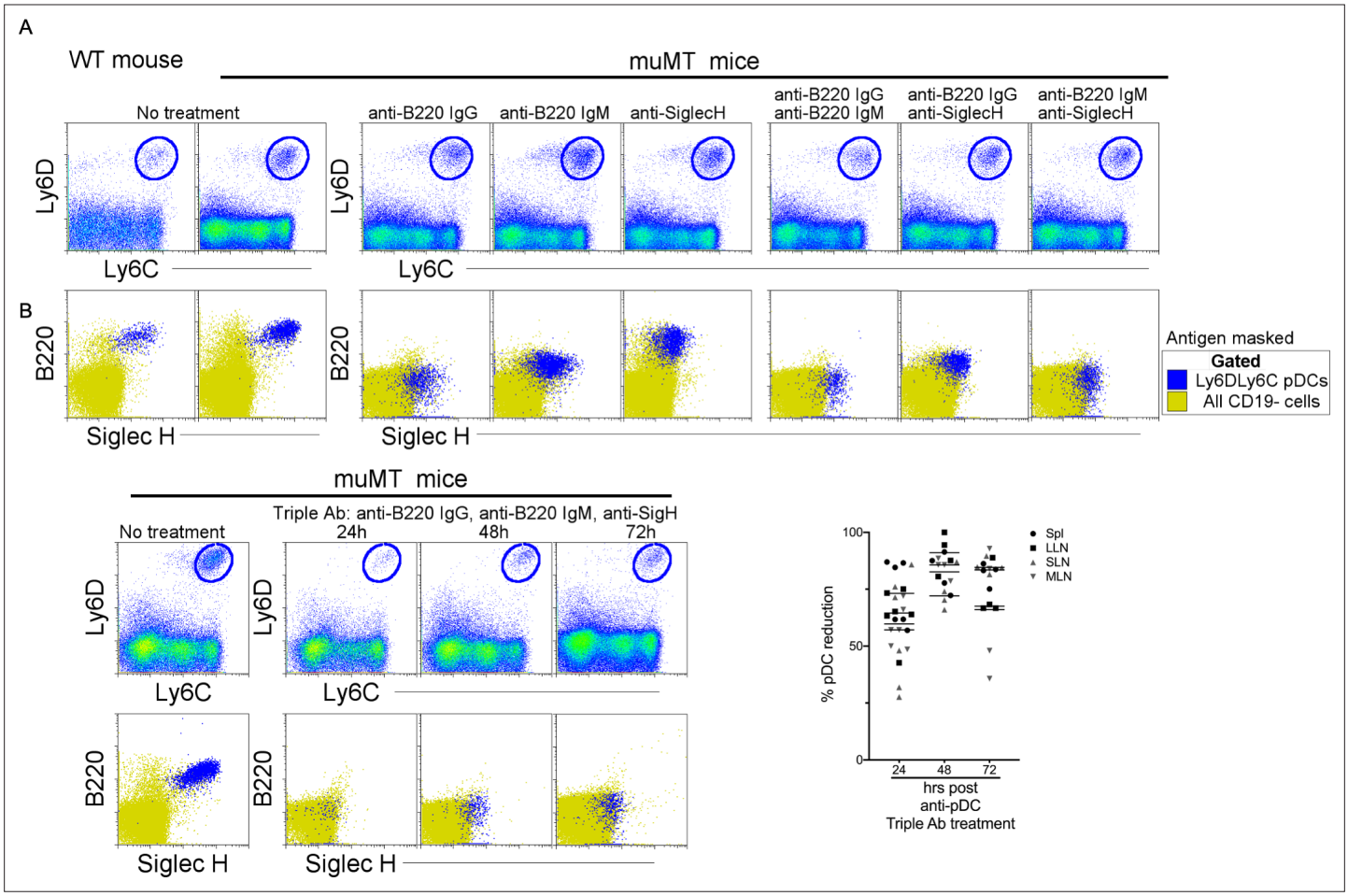

Figure 3—figure supplement 2. Depletion of the anti-tumor compensatory cell type, pDCs, in muMT mice. Three distinct monoclonal antibodies were tested for their capacity to deplete pDCs. Two of the antibodies are specific for B220: Rat anti-B220 IgG2a and Rat anti-B220 IgM; and one is specific for Siglec-H: Rat anti-Siglec-H IgG2b. The latter antibody is an isotype shared by other established depleting antibodies such as anti-CD4 (clone GK1.1) and anti-Gr1 (clone RB685C). (**A**) At high concentrations of 1 mg, none of the antibodies alone, or in combinations of two, depleted pDCs at 24 hr, instead the antibodies masked the targeted antigen as illustrated in flow plot overlays of pDCs identified by Ly6C and Ly6D from all splenic CD19 cells. Bottom row, flow cytometry overlays of all CD19 cells (yellow) and gated pDCs (blue) illustrate the masking of B220 and SiglecH 24 hr after muMT mice were ip injected, alone or in combination, with anti-mouse B220 rat IgG2a, anti-mouse B220 rat IgM, and anti-mouse Siglec-H. (**B**) However, when all three antibodies were given, pDCs were diminished by 63–83% in the spleen and LNs of muMT mice, and this depletion persisted across 24, 48, and 72 hr. Top row, gated $Ly6C^{+}Ly6D^{+}$ pDCs from all splenic CD19 cells. Bottom row, flow cytometry overlays of all CD19 cells (yellow) and gated pDCs (blue) illustrating the few cells remaining at 24, 48, and 72 hr after pDC-depleting triple antibody (Ab) treatment (anti-mouse B220 rat IgG2a, anti-mouse B220 rat IgM, and anti-mouse Siglec-H). Scatter plot represents four independent experiments, mean ± SEM. pDC, plasmacytoid dendritic cell.

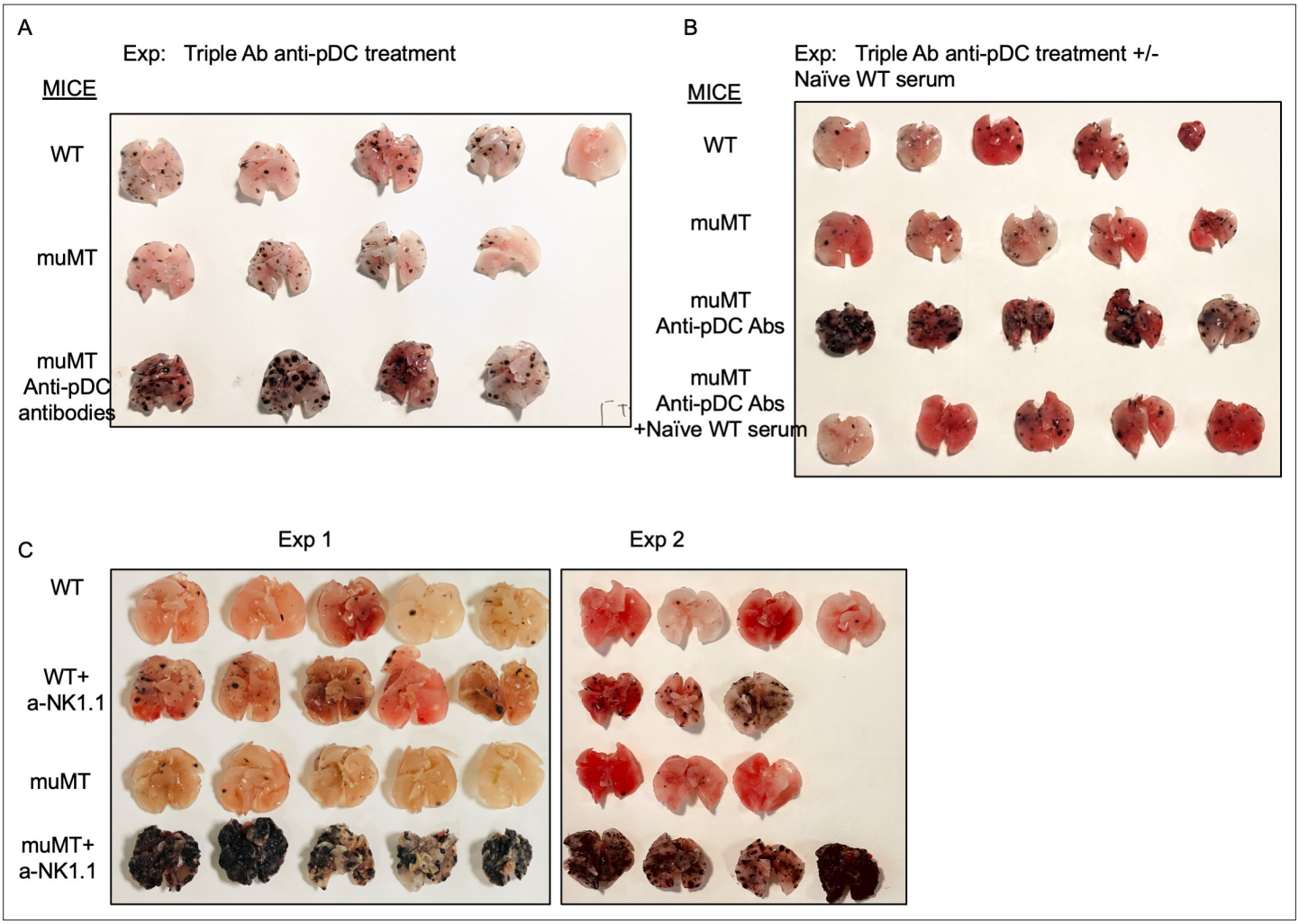

Figure 3—figure supplement 3. Anti-pDC treatment alone increased the tumor burden in muMT mice, but anti-pDC treatment given with naive WT serum reduces the tumor burden. Picture depicts agarose inflated lungs challenged with B16F10 melanoma in (**A**) WT, muMT, and pDC-depleted muMT; and (**B**) WT, muMT, pDC-depleted muMT, and pDC-depleted muMT injected with naive WT serum. (**A**) and (**B**) are two independent experiments. (**C**) Pics of mets per lung in WT and muMT mice with and without anti-NK1.1 treatment, scatter plot ***Figure 3E***. pDC, plasmacytoid dendritic cell; WT, wild-type.

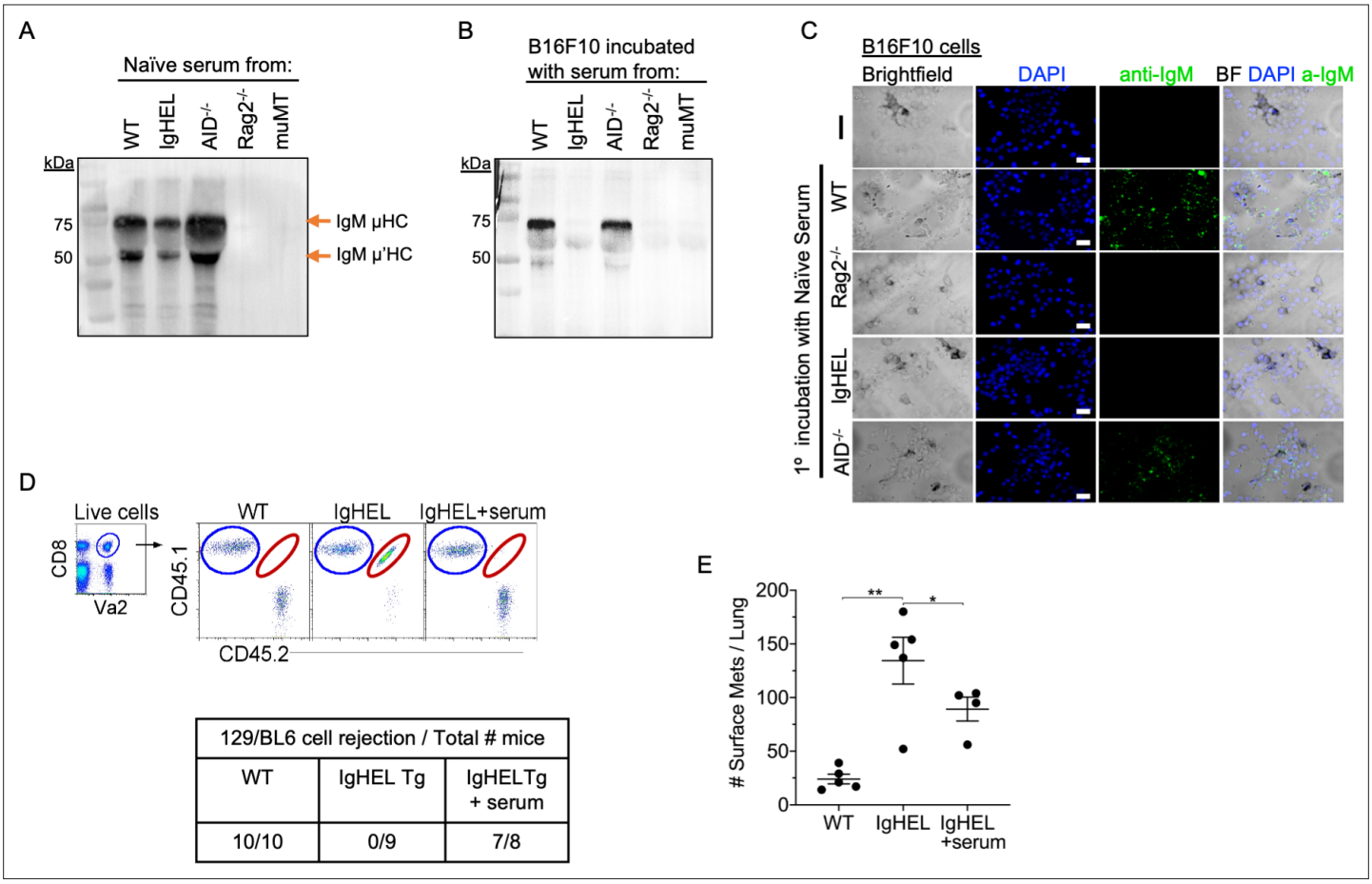

129/BL6 cell rejection / Total # mice		
WT	IgHEL Tg	IgHELTg + serum
10/10	0/9	7/8

Figure 4. Natural IgM repertoire tags neoantigen expressing cells for clearance. (**A**) Western blot IgM analysis of naive serum from WT, IgHEL, *Aicda*, *Rag2*$^{-/-}$, and muMT mice ***Figure 4—source data 1***. (**B**) B16F10 cells preincubated with naïve WT, IgHEL, *Aicda*, *Rag2*$^{-/-}$, and muMT serum, washed and run by Western blot for IgM analysis ***Figure 4—source data 1***. (**C**) Live B16F10 cells were plated on Lab-Teks slides and incubated with either naïve WT, *Rag2*$^{-/-}$, IgHEL, *Aicda*, and muMT serum or no serum, to detect IgM binding on cells (green). Scale bars, 40 µm. (**D**) *Experimental design* as in ***Figure 1A***. C57BL/6 WT, IgHEL, and IgHEL mice treated with serum were analyzed for the rejection of CD45.1/2 129BL6 cells. Table illustrates # rejected/mice examined. (**E**) Scatter plot illustrates the number of B16F10 induced surface mets in WT and IgHEL mice, each dot represents one mouse. *p<0.01, **p<0.003. WT, wild-type.